Journal of Alloys and Compounds 520 (2012) 59–64

Contents lists available at SciVerse ScienceDirect

Journal of Alloys and Compounds

journal homepage: www.elsevier.com/locate/jallcom

# Self-propagating high-temperature synthesis of nonstoichiometric wüstite

Maki Hiramoto[a], Noriyuki Okinaka[b], Tomohiro Akiyama[b,*]

[a] Graduate School of Engineering, Hokkaido University, Sapporo 060-8628, Japan
[b] Center for Advanced Research of Energy and Materials, Faculty of Engineering, Hokkaido University, Sapporo 060-8628, Japan

ARTICLE INFO

*Article history:*
Received 16 November 2011
Received in revised form
13 December 2011
Accepted 14 December 2011
Available online 11 January 2012

*Keywords:*
Self-propagating high-temperature synthesis
Nonstoichiometric oxides
Wüstite
Point defects
Crystal structure

ABSTRACT

This paper describes the self-propagating high-temperature synthesis (SHS) of nonstoichiometric $Fe_xO$ ($x = 0.833–1$), with particular focus on the effects of nonstoichiometric Fe content and diluent addition on the phase of the SHS product. In the SHS process, the raw materials Fe, $NaClO_4$ (oxidizer), and NaCl (diluent) were thoroughly mixed in the desired ratio by ball milling, and the lower surfaces of the disk-shaped green compacts were subsequently electrically ignited to produce $Fe_xO$ through the propagation of the sustainable exothermic reaction. X-ray diffraction analysis showed that the SHS products comprised double phases of $Fe_xO$ and $Fe_3O_4$. The peaks of products with $0.947 \leq x \leq 1.00$ shifted to lower angles in comparison to those of the product with $x = 0.833$ attributed to the lattice parameter distortion of the crystal structure because of the Fe defects. In the presence of the NaCl diluent, the raw materials were converted to high-purity $Fe_xO$ powders during the SHS process. Without the NaCl diluent, the lattice parameter of SHS $Fe_{0.947}O$ corresponded to the theoretical lattice parameter. Nonstoichiometric compounds of $Fe_xO$ ($0.942 \leq x \leq 0.952$) were obtained through SHS without additional external heating.


## 1. Introduction

It is well known that nonstoichiometric compounds have unique magnetic, electrical, thermal, optical, and mechanical properties owing to the effect of lattice vibrations [1,2]. Nonstoichiometric transition metal oxides such as $TiO_x$, $VO_x$, $Fe_xO$, $Mn_xO$, $Co_xO$, and $Ni_xO$ crystallize in the simple rock salt structure with varying degrees of intrinsic defects, typically present on the cationic sublattice. The aggregation of these intrinsic defects confers semiconductor properties on these nonstoichiometric oxides even without the addition of rare metal dopants.

Wüstite ($Fe_xO$) is one of the phases of iron oxide and is a well-known nonstoichiometric compound. The intriguing physical and chemical properties of $Fe_xO$ have garnered unflagging interest for more than 90 years on the basis of both practical and cognitive considerations. For instance, $Fe_xO$ is a major constituent of the oxide-scale formed on iron and iron-based alloys, and plays an important role in the reduction processes of iron ores. $Fe_xO$ is stable only at temperatures above 570 °C at atmospheric pressure; below 570 °C, $Fe_xO$ disproportionates into $Fe_3O_4$ and Fe [3]. $Fe_xO$ can also exist as a metastable phase at room temperature by quenching from high temperatures where $Fe_xO$ exists in the equilibrium state [4]. $Fe_xO$ exhibits relatively large deviation from stoichiometry depending on the temperature and the oxygen partial pressure, whereas the nonstoichiometric oxides $Co_xO$ and $Ni_xO$ have a limited range of possible nonstoichiometric states. The large nonstoichiometric range of $Fe_xO$ results in complicated electronic and ionic disorder. In addition, the defect and transport properties of $Fe_xO$ have been the subject of extensive experimental studies and theoretical considerations.

In addition to $Fe_xO$, other iron oxide phases are also of technological importance and have found a number of applications including use as recording materials, electrophotographic development agents [5], in catalysis, and as gas sensors [6]. Intensive investigations of the thermodynamic and structural properties as well as the electrical properties of the $Fe_xO$ system have been executed. These studies suggest that defect ordering within the $Fe_xO$ phase may be complex [7]. The unusual electronic properties of $Fe_xO$ including the fact that it is a semiconductor whose carrier type changes from p to n type around $x = 0.92$ [8] make $Fe_xO$ interesting in its own right.

Nonstoichiometric transition metal oxides are conventionally produced based on equilibrium. However, the conventional method suffers from the limitations of being time- and energy-consuming, because the raw materials must be kept at a high temperature for an extended period in order to reach the equilibrium compositions of the products [3].

In order to obviate the drawbacks associated with the conventional production of $Fe_xO$, we applied self-propagating high-temperature synthesis (SHS) as an alternative production method [9]. This method harnesses the thermal energy generated by an exothermic chemical reaction between metal powders and an

* Corresponding author. Tel.: +81 11 706 6842; fax: +81 11 726 0731.
*E-mail address:* takiyama@eng.hokudai.ac.jp (T. Akiyama).

0925-8388/$ – see front matter © 2011 Elsevier B.V. All rights reserved.
doi:10.1016/j.jallcom.2011.12.057

**Table 1**
Properties of raw materials used for synthesizing $Fe_xO$ ($x = 0.833–1$) by SHS.

| Raw materials | Source | Particle diameter (μm) | Purity (mass%) |
|---|---|---|---|
| Fe | Kojundo Chemical | 3–5 | 99.9 |
| $NaClO_4$ | Aldrich | >10 | 98 |
| NaCl | Kojundo Chemical | >10 | 99.9 |

oxidant comprised of various raw materials to generate the desired product. The principle of SHS is that once one end of the starting mixture is ignited, an exothermic sustainable reaction initiates and causes a combustion wave to propagate through the sample, and the desired product is finally generated without additional energy [10,11]. In addition to saving energy, SHS offers several benefits including minimization of the operating time, simplification of procedure and equipment, and facile control of the composition of the product by methodical variation of the molar ratio of the raw materials [12,13].

To the best of our knowledge, there are no published reports on SHS of nonstoichiometric $Fe_xO$, despite its scientific significance. Therefore, the purpose of this study was to synthesize nonstoichiometric $Fe_xO$ ($0.833 \leq x \leq 1.00$) using the SHS method, focusing on the effects of the nonstoichiometric Fe content and diluent addition on the phase of the SHS product. The findings of this study are expected to pave the way for a new $Fe_xO$ production route with the benefits of energy saving and minimized production time.

## 2. Experimental

The properties and sources of the raw materials used for the synthesis of $Fe_xO$ ($0.833 \leq x \leq 1.00$) are listed in Table 1. $NaClO_4$ was selected as an oxidizing reagent for metallic iron [10]. Note that NaCl was added to the raw materials as a diluent to provide the effect of decreasing the adiabatic flame temperature.

Fig. 1 shows the process flow sheet for the synthesis of $Fe_xO$ via the SHS method. First, Fe, $NaClO_4$, and NaCl powders were mixed in the desired ratio to obtain a total mass of 20 g. The mixture was then ball-milled in a 140 mm diameter alumina pot containing 25 alumina balls of 10 mm diameter. The mill was operated at 60 rpm for 3 h under atmospheric conditions. After the milling process, 10 g of the sample was pressed into a disk of 20 mm in diameter at 20 MPa for 10 min using a uniaxial single-acting press. Fig. 2 shows the schematic diagram of the experimental apparatus used for the SHS. The apparatus includes a reactor, a control unit, and a gas control system [12]. The green compact of the sample was placed into a graphite crucible with dimensions of 40 mm × 25 mm × 120 mm, and a disposable carbon foil (5 mm × 200 mm × 0.1 mm) used as an igniter was also placed in contact with the lower surface of the sample. Prior to commencing the reaction, the reactor was evacuated using a rotary pump and then filled with argon gas of 99.999% purity at atmospheric pressure. The sample was ignited by an electrically heated carbon foil for 5 s. After completion of the ignition process, the exhaust valve of the reactor was kept open for 20 min to allow the sample to cool down completely. The cooled sample was subjected to ultrasonic cleaning to remove NaCl and was dried overnight at 110 °C. The product was separated to retrieve the fraction with sizes less than 25 μm and the morphology was observed using scanning electron microscopy (SEM). The remaining product was ground in an agate mortar to obtain particles with sizes less than 25 μm. The phase of the product obtained was identified by powder X-ray diffraction (XRD) using Cu Kα radiation (λ = 1.5418 Å).

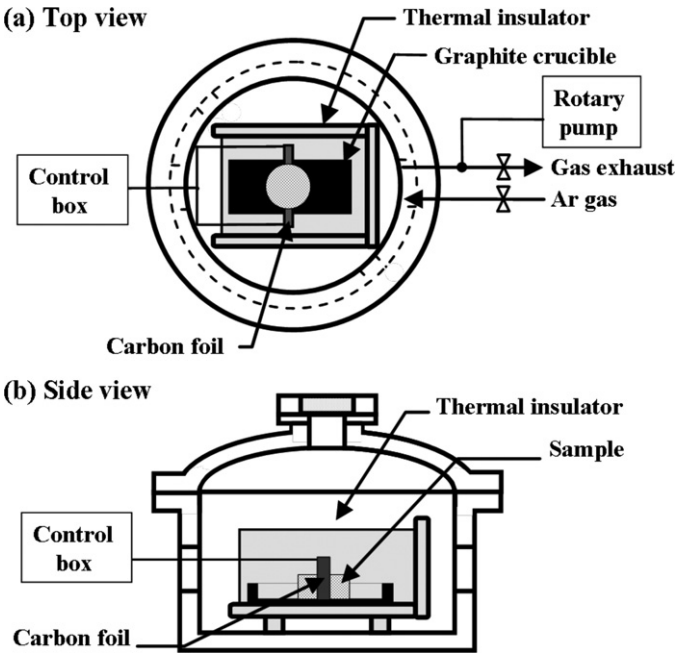


**Fig. 2.** Schematic diagram of the experimental apparatus for self-propagating high-temperature synthesis.

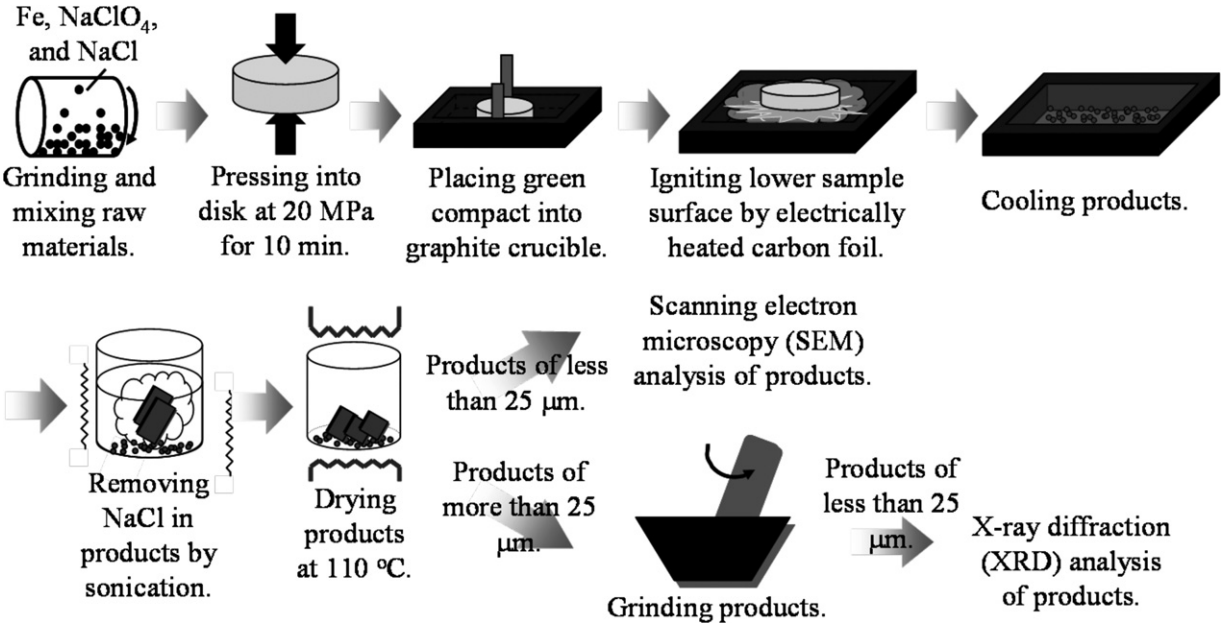


**Fig. 1.** Schematic illustration of SHS procedure.

**Table 2**
Molar specific heat of product materials $Fe_{0.947}O$ and NaCl.

| Product | Specific heat, $C_p$ (J mol$^{-1}$ K$^{-1}$) $C_p = A + B \times 10^{-3}\,T + C \times 10^{5}\,T^{-2} + D \times 10^{-6}\,T^{2}$ | | | | Temperature range (K) |
|---|---|---|---|---|---|
| | *A* | *B* | *C* | *D* | |
| $Fe_{0.947}O$ | 48.794 | 8.372 | −2.891 | 0 | 298.15–1650 |
| | 65.839 | 0 | 0 | 0 | 1650– |
| NaCl (g) | 37.56 | 0.383 | −1.715 | 0.217 | 298.15–3600 |

## 3. Results and discussion

The reaction involved in the SHS of $Fe_{0.947}O$ is given as follows:

$$0.947Fe + 0.25NaClO_4 = Fe_{0.947}O + 0.25NaCl(g) + 212.7\,kJ \quad (1)$$

The SHS process is only effective for strongly exothermic chemical reactions. An important parameter in this regard is the adiabatic flame temperature, $T_{ad}$, which was calculated using the following equation:

$$\int_{298.15}^{T_{ad}} \left( \sum_i n_i C_{ip} \right) dT = -\Delta H_r^{\circ} \quad (2)$$

Table 2 indicates the molar specific heat of the products in Eq. (1) for evaluating the $T_{ad}$ from the heat balance of SHS due to the iron oxidation, as given by Eq. (2). The data of Table 2 were referred to the HSC 5.11 thermodynamic software. $T_{ad}$ evaluated for the synthesis of $Fe_{0.947}O$ was 2042 K, which is above the melting point of $Fe_{0.947}O$ (1651 K).

Fig. 3(1) shows the overall SEM image of the SHS-generated $Fe_{0.947}O$ crystals with sizes less than 25 μm. Within this figure, SHS $Fe_{0.947}O$ particles with spherical morphology of various dimensions can be observed (Fig. 3(2a, 2b)) as well as SHS $Fe_{0.947}O$ products having an irregular shape (Fig. 3(3)). These particles are shown at higher magnification in the respective segments of Fig. 3 for clarity. The SEM observations suggest that the spherical micron-sized products crystallized from melted droplets because the $T_{ad}$ was sufficiently higher than the melting point of the products. As shown in Fig. 3(2b), the size of the product was smaller than that of raw materials. This may be due to the presence of the added NaCl. It is recognized that nanosized materials can be generated by an SHS method known as alkali metal molten salt assisted combustion [14]. The reduced dimensions of the products generated herein may stem from the fact that these products were produced in the molten NaCl. The submicron products were thus obtained after removal of NaCl in water. The irregularly shaped SHS $Fe_{0.947}O$ particles were produced by melting and sintering.

The SHS reaction for the formation of $Fe_xO$ is expressed by the following equation:

$$xFe + 0.25NaClO_4 \rightarrow Fe_xO + 0.25NaCl(g),\ (x = 0.833–1.00) \quad (3)$$

Fig. 4(a) shows the powder XRD patterns of the SHS $Fe_xO$ ($x = 0.833$–$1.00$) samples. All the $Fe_xO$ samples corresponded to the $Fe_xO$ and $Fe_3O_4$ phase. The value of $x$ exerted no significant effect on the phase of the products. The defect clusters of nonstoichiometric transition metal oxides consist of cation vacancies, cation

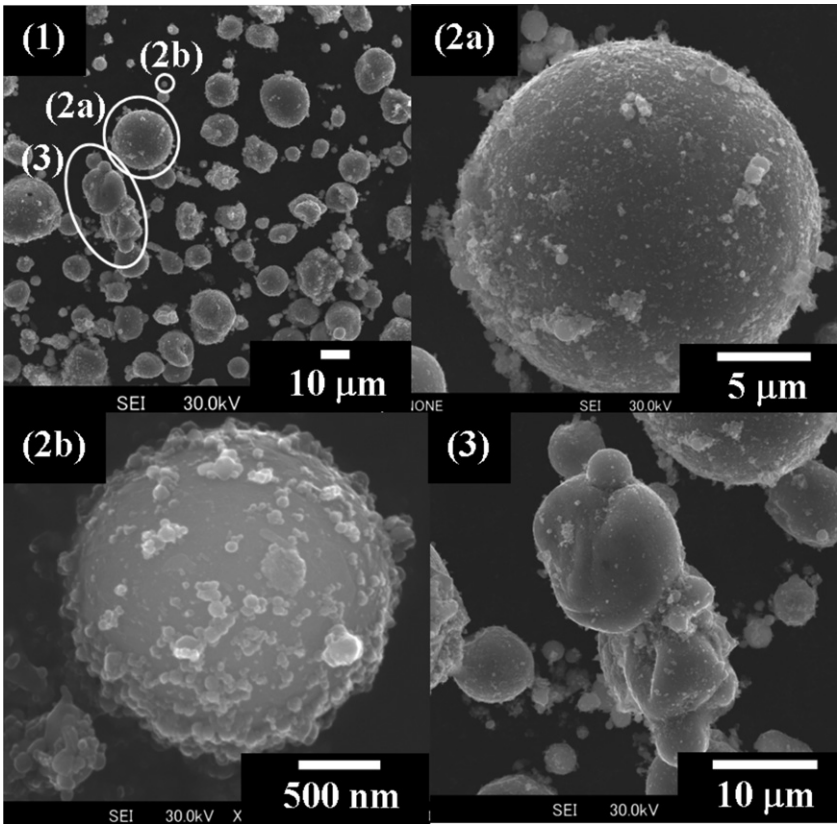


**Fig. 3.** SEM images of (1) SHS $Fe_{0.947}O$ crystals with sizes less than 25 (m and $Fe_{0.947}O$ with (2a, 2b) spherical shape of different sizes, and (3) irregular shape.

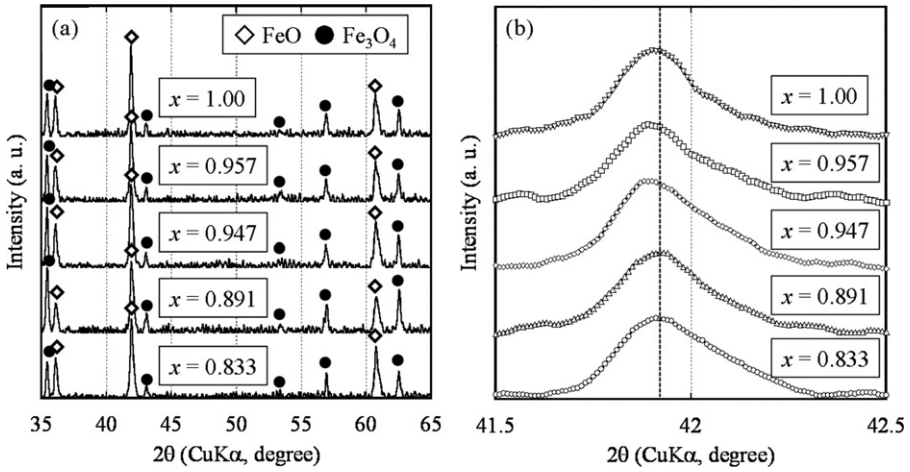


**Fig. 4.** (a) XRD patterns of $Fe_xO$ ($x$ = 0.833–1.00) synthesized by SHS method. The reaction involved in the SHS of $Fe_xO$ is given as follows: $x$Fe + 0.25$NaClO_4$ → $Fe_xO$ + 0.25NaCl (g) ($x$ = 0.833–1.00). (b) Enlargement of XRD patterns of SHS $Fe_xO$ in 2$\theta$ region of 41.5–42.5°.

interstitials, and holes. The simplest cluster is the so-called 4:1 cluster, which consists of 4 cation vacancies, 1 cation interstitial, and a variable number of holes. The 16:5 cluster formed by the aggregation of 4:1 clusters is an element of the inverse spinel structure typical of $Fe_3O_4$ [7]. Therefore, a product with large nonstoichiometric value tends to have a high $Fe_3O_4$ content. However, the XRD data indicate that there is no difference in the $Fe_3O_4$ content with decreasing $x$. This may be indicative of the fact that product generation is dependent on the adiabatic flame temperature and cooling rate.

Fig. 4(b) shows the enlarged XRD patterns ($41.5^\circ < 2\theta < 42.5^\circ$) of $Fe_xO$ ($x$ = 0.833–1.00) samples synthesized by the SHS method. The peaks of the products with $0.947 \leq x \leq 1.00$ shifted to lower angles in comparison to that of the product with $x$ = 0.833. This was attributed to the lattice parameter distortion of the crystal structure because of the Fe defects.

Table 3 displays the results of the quantitative estimation, the lattice parameter, and the calculated composition $x$ of $Fe_xO$ in the case where the experimental composition of Fe in the raw material was varied. The experimental composition ($x_{expt}$) is the ratio of the Fe content in the raw materials. The lattice parameter, $a_{experimental}$, was calculated from the following equation:

$$\frac{1}{d^2} = \frac{h^2 + k^2 + l^2}{a^2_{experimental}} \quad (4)$$

The following equation was used to calculate the composition $x$ of $Fe_xO$ from the lattice parameter, $a$ [3]:

$$a = 3.856 + 0.478x \quad (5)$$

The results showed that the products obtained contained approximately 70% $Fe_xO$. The theoretical lattice parameters ($a_{theoretical}$) were obtained by substituting the experimental composition into Eq. (5). The $a_{experimental}$ value tended to decrease as the experimental composition of Fe in the raw material decreased.

**Table 3**
Quantitative estimation of composition and lattice parameter of SHS $Fe_xO$ product from XRD patterns.

| $x_{expt}$ | $Fe_xO$ content (%) | $Fe_3O_4$ content (%) | $a_{theoretical}$ (Å) | $a_{experimental}$ (Å) | $x_{calc}$ |
|---|---|---|---|---|---|
| 0.833 | 78 (±4) | 22.2 (±1.3) | 4.254 | 4.307 | 0.944 |
| 0.891 | 59 (±2) | 40.6 (±1.8) | 4.282 | 4.306 | 0.942 |
| 0.947 | 72 (±2) | 28.3 (±1.4) | 4.309 | 4.309 | 0.947 |
| 0.957 | 72 (±3) | 28.1 (±1.6) | 4.313 | 4.310 | 0.950 |
| 1.00 | 73 (±2) | 26.6 (±1.1) | 4.334 | 4.311 | 0.952 |

This methodical variation of the molar ratio of the raw materials showed that in the case of $x_{expt}$ = 0.947, the calculated composition ($x_{calc}$) was coincident with the experimental composition.

The reaction involved in SHS of $Fe_{0.947}O$ with/without NaCl diluent is given as follows:

$$(0.947–3.788z)Fe + (0.25–z)NaClO_4 + zNaCl \rightarrow (1–4z)Fe_{0.947}O + 0.25NaCl, \quad (z = 0 \text{ or } 0.05) \quad (6)$$

$T_{ad}$ evaluated for the SHS reaction with the addition of the NaCl diluent was 1805 K. The SHS reaction was not self-sustaining when more than 5 mol% NaCl diluent was utilized. This suggested that the addition of more than 5 mol% diluent caused extinction of the reaction without sufficient generation of self-propagating heat. In general, empirical evidence indicates that reactions are not self-sustaining when $T_{ad}$ is less than 1800 K [15].

Fig. 5(a) shows the XRD patterns of the $Fe_{0.947}O$ sample produced by SHS with/without NaCl diluent. Only $Fe_xO$ and $Fe_3O_4$ phases were detected without the addition of the diluent. In contrast, upon addition of the NaCl diluent, un-reacted Fe was also detected in addition to the $Fe_xO$ and $Fe_3O_4$ phases. This suggested that the contact area of the reactants decreased because of the addition of diluent. It was also observed that the intensity of the $Fe_3O_4$ peak was decreased in product prepared with diluent with accompanying increase in the intensity of the $Fe_xO$ peak, in comparison to the product prepared without diluent.

Fig. 5(b) shows the enlarged XRD patterns of the $Fe_{0.947}O$ sample produced by SHS with/without NaCl diluent in the 2$\theta$ range of 41.5–42.5°. This peak was coincident for the products obtained with and without NaCl diluent.

Table 4 displays a comparison of the quantitative estimation, the lattice parameter, and the calculated composition $x$ of $Fe_xO$ for the SHS products obtained with and without diluent. In the case of diluent addition, the content of $Fe_3O_4$ impurity decreased, and the purity of $Fe_xO$ was improved by more than 10%. This may be accounted for by the decrease in the adiabatic flame temperature and wave velocity generated by addition of the diluent, resulting in a homogenous reaction with a narrow reaction zone [16]. Therefore, the reactivity increases under these conditions and a higher purity of $Fe_xO$ was obtained. However, the calculated composition of the product prepared with the diluent shows a slight deviation from the experimental composition of 0.947.

Fig. 6(a) shows the relationship between the experimental and calculated composition of SHS $Fe_xO$ without NaCl diluent; the calculated values are indicated next to the data points. The

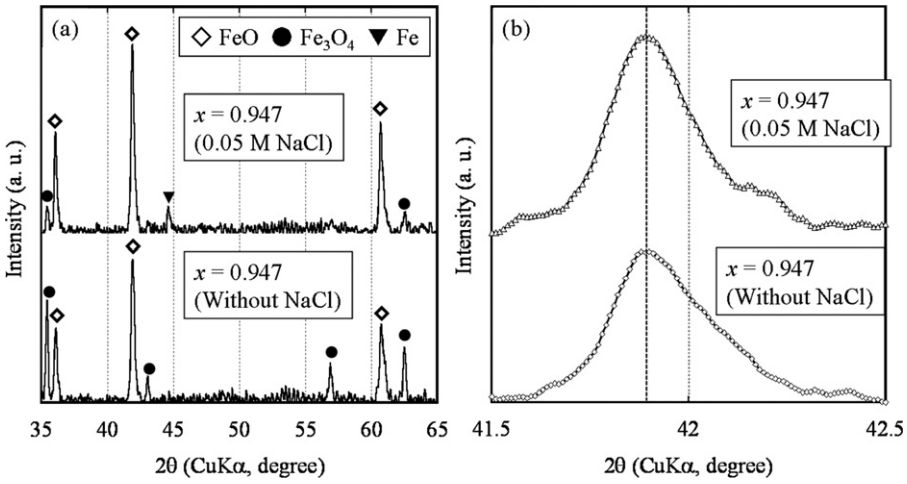


**Fig. 5.** (a) XRD patterns of the $Fe_{0.947}O$ sample produced by SHS with/without NaCl diluent, in which the synthesis reaction is expressed by the following equation: $(0.947–3.788z)Fe + (0.25–z)NaClO_4 + zNaCl \rightarrow (1–4z)Fe_{0.947}O + 0.25NaCl$ ($z = 0$ or 0.05). (b) Enlarged areas of the spectra in (a) from $2\theta = 41.5–42.5^\circ$.

**Table 4**
Quantitative estimation of composition and lattice parameter of the SHS $Fe_{0.947}O$ with/without NaCl diluent from XRD patterns.

| $x_{expt}$ | Content of $Fe_xO$ (%) | Content of $Fe_3O_4$ (%) | Content of Fe (%) | $a_{theoretical}$ (Å) | $a_{experimental}$ (Å) | $x_{calc}$ |
|---|---|---|---|---|---|---|
| 0.947 (0 M NaCl) | 72 (±2) | 28.3 (±1.4) | – | 4.309 | 4.309 | 0.947 |
| 0.947 (0.05 M NaCl) | 86 (±3) | 10.3 (±1.0) | 3.7 (±0.6) | 4.309 | 4.311 | 0.952 |

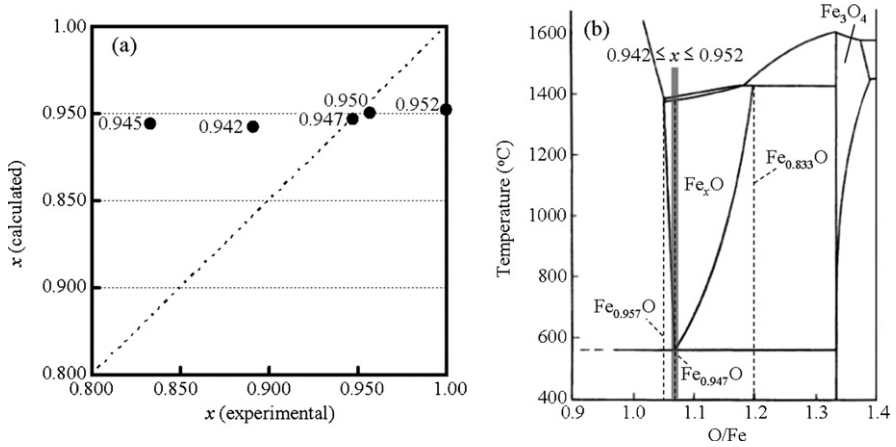


**Fig. 6.** (a) Relationship between experimental and calculated composition of SHS $Fe_xO$ without NaCl diluent. The calculated values are indicated next to the data points. The experimental composition $x$ is the ratio of the Fe content in the raw materials. The following equation was used to calculate the composition $x$ of $Fe_xO$ from $a$, the lattice parameter: $a = 3.856 + 0.478x$ [3]. (b) Phase diagram for the Fe–O system [17]. Nonstoichiometric compounds of $Fe_xO$ ($0.942 \leq x \leq 0.952$) were obtained through SHS without additional external heating.

composition of SHS $Fe_xO$ was limited to a narrow nonstoichiometric range. Fig. 6(b) shows the phase diagram for the Fe–O system [17]. The shaded region shows the composition range obtained by SHS, and the stoichiometric composition of wüstite is generally accepted to be $x = 0.947$. The nonstoichiometric compounds of SHS $Fe_xO$ were obtained within the composition range of $x = 0.942–0.952$, which are of the ±0.005 limits of the stoichiometric composition of 0.947.

## 4. Conclusions

The effects of nonstoichiometric content and diluent addition on the self-propagating high-temperature synthesis (SHS) of nonstoichiometric $Fe_xO$ ($x = 0.833–1.00$) were experimentally evaluated. The following results were obtained:

(1) All of the products obtained were double phases of $Fe_xO$ and $Fe_3O_4$. The $Fe_xO$ peaks of products with $0.947 \leq x \leq 1.00$ shifted to lower angles in comparison to that of the product with $x = 0.833$. This shift was caused by the presence of lattice defects.
(2) The addition of a NaCl diluent to the raw material mixture during SHS facilitated the conversion of the raw materials to yield high-purity $Fe_xO$ powders.
(3) The lattice parameter of $Fe_{0.947}O$, synthesized by SHS without NaCl diluent, corresponded to the theoretical lattice parameter. Nonstoichiometric compounds of $Fe_xO$ ($0.942 \leq x \leq 0.952$) were obtained through SHS without additional external heating.

The results reveal that the SHS method can be used to produce nonstoichiometric $Fe_xO$ with the benefits of energy saving and minimization of production time. The purity of $Fe_xO$ obtained by this method may be further improved by magnetic separation of $Fe_3O_4$ and Fe.

## References

[1] M. Jiménez-Melendo, A. Domínguez-Rodríguez, J. Castaing, Acta Metall. Mater. 43 (1995) 3589–3604.
[2] R. Aragón, Phys. Rev. B 46 (1992) 5328.
[3] C.A. McCammon, L.-G. Liu, Phys. Chem. Miner. 10 (1984) 106–113.
[4] Y. Masaki, T. Fujii, M. Hayashi, K. Nagata, ISIJ Int. 51 (2011) 203–207.
[5] Y.B. Khollam, S.R. Dhage, H.S. Potdar, S.B. Deshpande, P.P. Bakare, S.D. Kulkarni, S.K. Date, Mater. Lett. 56 (2002) 571–577.
[6] G. Neri, A. Bonavita, S. Galvagno, P. Siciliano, S. Capone, Sens. Actuators B: Chem. 82 (2002) 40–47.
[7] S. Mrowec, A. Podgórecka, J. Mater. Sci. 22 (1987) 4181–4189.
[8] D.P. Johnson, Solid State Commun. 7 (1969) 1785–1788.
[9] H.C. Yi, J.J. Moore, J. Mater. Sci. 25 (1990) 1159–1168.
[10] H. Ishikawa, K. Oohira, T. Nakajima, T. Akiyama, J. Alloys Compd. 454 (2008) 384–388.
[11] K. Taniguchi, N. Okinaka, T. Akiyama, J. Alloys Compd. 509 (2011) 4084–4088.
[12] T. Hirano, H. Purwanto, T. Watanabe, T. Akiyama, J. Alloys Compd. 441 (2007) 263–266.
[13] I.S. Ahmed, S.A. Shama, H.A. Dessouki, A.A. Ali, Mater. Chem. Phys. 125 (2011) 326–333.
[14] S.T. Aruna, A.S. Mukasyan, Curr. Opin. Solid State Mater. Sci. 12 (2008) 44–50.
[15] Z.A. Munir, U. Anselmi-Tamburini, Mater. Sci. Rep. 3 (1989) 277–365.
[16] H. Jie-Cai, X.-H. Zhang, J.V. Wood, Mater. Sci. Eng. A 280 (2000) 328–333.
[17] B. Sundman, J. Phase Equilib. 12 (1991) 127–140.